Applied Ocean Research 138 (2023) 103649

Contents lists available at ScienceDirect

Applied Ocean Research

journal homepage: www.elsevier.com/locate/apor

On the three-dimensional effects of the water entry of wedges

Xueliang Wen, Muk Chen Ong, Guang Yin *

Department of Mechanical and Structural Engineering and Materials Science, University of Stavanger, Stavanger, Norway

ARTICLE INFO

Keywords:
Water entry
Wedge
Three-dimensional effect
Modeling

ABSTRACT

Three-dimensional (3D) effects on the total and spanwise slamming coefficients and the pressure reductions acting on the wedge surface during water entry are modeled in a unified manner. First, the water entry of wedges with a constant speed is numerically studied using the finite volume method (FVM) combined with the volume of fluid (VOF) method. The wedge is assumed to enter water with high speeds such that the compressibility, viscosity, gravity and surface tension effects of the fluid can be neglected. The numerical method is validated against an experimental measurement of a freefall water entry of a wedge with a deadrise angle of 30°. Then, the water entry of 3D wedges with deadrise angles of 30, 35, 40 and 45° and beam-span ratios between the width and length varying from 0 to 1 are simulated. The total and spanwise slamming coefficients and the reduction of the pressure distribution are analyzed. The total slamming coefficient is derived with a 3D effect coefficient using a dimensional analysis in the slamming stage and its expression for the transition stage is proposed based on a two-dimensional (2D) transition stage model of the water entry. The spanwise slamming coefficients on the different spanwise sections are modeled with the pressure coefficient distribution of a supercavitating flow around a 2D flat plate. The reductions of the pressure acting on the wedge surface are found to be approximately constant along the wetted length for all spanwise sections, which can be derived using the expressions of the total and spanwise slamming coefficients. Finally, using the proposed model, the predictions of the abovementioned variables are in good agreement with the numerical simulation results in the slamming and transition stages during the water entry of the wedges with different deadrise angles and beam-span ratios.

1. Introduction

Water entry problems play an important role in ship slamming (Faltinsen, 2005; Kapsenberg, 2011), the high-speed planing of hulls (Savitsky, 1964; Savitsky et al., 2007) and water landing of seaplanes (Garme, 2005; Smiley, 1950). For most of the marine structures, the body shapes are usually three-dimensional (3D). The impact flow of the water entry of a 3D body is more complicated than that of a two-dimensional (2D) body, such as a flat plate and circular cylinder with an infinite spanwise length. In the original studies of water entry, 2D models were commonly used to compute the hydrodynamic forces and the pressure distributions on the body surface theoretically. The results of the 2D theoretical models cannot be used for the water entry of 3D bodies without corrections. Strip theory (Garme, 2005) and 2D+t theory (Sun and Faltinsen, 2007, 2012) are classical methods that are used to extend the 2D water entry models from 2D cases to 3D cases. The slamming forces are calculated as the sum of hydrodynamic forces acting on the 2D sections with longitudinal thickness during the 2D water entry of these sections. Due to the turbulent nature of the flow around the vessel and the significant variation in hull shape, the 2D+t theory works better than the strip theory, particularly in the front portion where slamming phenomenon occurs. However, in the 2D+t theory, the reductions of the hydrodynamic forces (compared with those of the 2D water entry) due to the 3D flows near the ship bow and stern are rarely considered. The reductions of hydrodynamic forces and pressure acting on the body surfaces are named as 3D effects of the water entry. Without considering the 3D effects, the 3D models will have errors when performing the simulations of the dynamic responses of the ship to different sea states and loading conditions on rough seas. Beside, the experiments of the water entry of hull segments (Xie et al., 2019, 2018) are conducted before the real ships are launched into the water (Zhao et al., 1996; Wu et al., 2004; Yettou et al., 2006; Luo et al., 2012). This kind of experiments are performed to evaluate the slamming forces acting on the ship when it is sailing on the rough seas. The full-scale model of a complete ship is not used for slamming experiments because of the high experimental cost. The segment of the ship itself will induce significant 3D effects when its segment length is too short

* Corresponding author.
E-mail address: guang.yin@uis.no (G. Yin).

https://doi.org/10.1016/j.apor.2023.103649
Received 31 March 2023; Received in revised form 27 May 2023; Accepted 24 June 2023
Available online 30 June 2023

Nomenclature

A, B	parameters of the quadratic function of the 3D effect coefficient
a, b	parameters of the quadratic function of h_2
A_0	auxiliary variable of the supercavitating flow around a 2D wedge
c	wetted length
C_{const}	dimensionless coefficient of the water entry of a 2D wedge
C_p	pressure coefficient
c_q	volume fraction of q^{th} fluid
C_s	slamming coefficient of a 3D water entry
C_{s2}	slamming coefficient of a 2D water entry
C_{s2max}	maximum C_{s2} of a 2D water entry
C_{smax}	maximum C_s of a 3D water entry
$C_{s2\infty}$	C_{s2} of a supercavitating flow around a 2D wedge
$C_{s\infty}$	C_s of a supercavitating flow around a 3D wedge
$C^*_{s\infty}$	auxiliary variable of the present transition stage model
$C_{s\infty min}$	minimum $C_{s\infty}$ of a supercavitating flow around 3D wedges in $l/L \in [0,\ 1]$
C^*_s	dimensionless variable related to C_s of the transition stage
C_{sz}	spanwise slamming coefficient
C_{szmax}	maximum spanwise slamming coefficient
C_{sz0max}	maximum spanwise slamming coefficient of the centre section
f	dimensionless function for the pressure coefficient
F	force acting on bodies in the vertical direction
g	body force vector
h	penetration depth
h_2	penetration depth corresponding to C_{smax}
h_{2z}	penetration depth corresponding to C_{szmax}
h^*	penetration depth corresponding to $(h - h_2)/h_2\cot^{1.3075}\beta$
k_1	dimensionless penetration depth of the maximum C_s
l	half width of the wedge
L	spanwise length of a 3D wedge
p	pressure
p_a	atmosphere pressure
t	time
t_{end}	end time of simulation
U_0	entering speed of a wedge on the water
U_w	instantaneous speed of the wedge
V_q	velocity vector of the q^{th} fluid
V	velocity vector of fluid
x, y, z	Cartesian coordinates
β	deadrise angle of wedge bodies
Δt	time-step
ΔC_p	reduction of C_p in the slamming stage
γ	correction factor of wetted length
λ	parameter of the transition stage model
κ	correction function of a near-transom load model
Ψ	3D effect coefficient
ρ	density of water
τ, τ_0	auxiliary variable of the supercavitating flow around a 2D wedge
θ	C_{sz} distribution along the spanwise direction
θ^*	C_p distribution of the supercavitating flow around a 2D flat plate
Θ	auxiliary function related to the integral of θ along the spanwise direction

Subscript

q	phase of fluid

compared with the beam of the ship. The 3D effects will lead to underestimated slamming loads on the ship segment, which cannot accurately reproduce the slamming loads acting on the real ship during the sailing on the rough seas. The 3D corrections of the slamming loads from the experiments should be conducted using the theories of the 3D effects of water entry. Summarized from the two abovementioned research scenarios, there is an increasing need to study the 3D effects for the water entry of bodies. Furthermore, it is also necessary to provide a model for the 3D effect corrections for the strip theory or 2D+t theory and the experimental results of the water entry of ship segments. In the present study, the high-speed water entry of wedges is investigated and the 3D effects of the water entry problems will be theoretically analyzed. For the sake of simplicity, under the high-speed impact assumption, the water entry is considered to be gravity-free, which is also used in the original theoretical studies of Von Karman (1929), and Wagner (1932).

The 3D effects of water entry problems depend on the water entry stages where the free surfaces have different forms. The whole duration of the water entry can be generally divided into four successive stages according to the experimental observations of Wang et al. (2015):

(a) Slamming stage. The hydrodynamic force acting on the wedge surface increases rapidly with the increasing penetration depth until the spray root of the impact flow reaches the knuckle of the wedge. A new free surface is formed when the jet tip exceeds the knuckle of the wedge, but the separation of jet has a negligible effect on the pressure and hydrodynamic force acting on the wedge surface (Zhao and Faltinsen, 1991).
(b) Transition stage. The spray root exceeds the knuckle of the wedge. The high pressure near the spray root declines dramatically because the wall surface no longer forces against the water bulk of the spray root. The new free surface near the wedge continues to extend, but its horizontal velocity becomes smaller and the cavity above the wedge is formed.
(c) Collapsed stage. The new free surface collapses to the centre of the cavity because of its inward horizontal velocity caused by the effect of the gravity on the water. The cavity is stretched and the free surfaces on both sides approach each other.
(d) Post-closure stage. The upper part of the free surfaces of both sides impact on each other and the cavity is closed like a pinch-off. The vertical velocity of the water above the pinch-off point is very large and a high-speed water column is formed.

The collapsed and post-closure stages result from the effect of the gravity on the water when the entering speed of wedge is not large. For a high-speed water entry, the last two stages can be neglected and the slamming and transition stages play the most important role during the water entry of bodies.

The theoretical studies on the slamming and transition stages mainly focus on the 2D gravity-free water entry of bodies. For the slamming stage, Von Karman (1929) contributed to the primitive theoretical work for the hydrodynamic force using an added mass method. Wagner (1932) proposed the first complete theory including the modeling of the free surface deformation, the pressure distribution on the body surface and the hydrodynamic force. The Wagner theory was further developed into matched asymptotic expansions by Howison et al. (1991) and other sophisticated asymptotic theories of Korobkin (2004). Compared with the asymptotic theories, the self-similarity solutions developed by Dobrovol'skaya (1969) and Semenov and Iafrati (2006) are the fully nonlinear solutions and are thus the most accurate models for the water entry of wedges with a constant speed. These similarity solutions are widely used to provide the hydrodynamic force and pressure distribution for benchmarks of numerical methods (Zhao et al., 1996; Wen et al.,

2021) and experimental results (Greenhow and Lin, 1983). For the transition stage, Tassin et al. (2014) proposed a liner fictitious body continuation (FBC) based on the asymptotic theories of Korobkin (2004) to model the transition stage of the water entry. Wen et al. (2022) improved Tassin et al. (2014) method proposing a curved FBC, which can accurately predict the hydrodynamic force and pressure distribution for the water entry in a constant speed. The complete models including the slamming and transition stages, and the cases of constant and varying speeds are developed by Wen et al. (2022) using the theoretical results of the similarity solution (Dobrovol'skaya, 1969) and the supercavitating flow around a 2D wedge (Korvin-Kroukovsky and Chabrow, 1948; Gurevich, 1965). The abovementioned solutions can be used to extend to the gravity-free water entry of 3D wedges considering the 3D effects. The studies of Zekri et al. (2021) and Sun et al. (2015) revealed that the gravity of the water will increase the hydrodynamic force and the pressure in the central part of the wetted region. However, the gravity effects are relatively small for the initial stage of the water entry. The gravity effects will become significant with time for the later stages. In the present study, we focus on the modeling of the gravity-free water entry under 3D effects for the high-speed impact problems.

The research on the 3D effects of the water entry of wedges can be mainly categorized into three branches. The first branch is the modeling of the hydrodynamic force reductions for different beam-span ratios. The modeling of the hydrodynamic force reductions is proposed based on the added mass of a thin rectangular plate. Pabst (1930) proposed the first formula of the 3D effect coefficient based on the experimental measurements of the added mass of a flat plate. The 3D effect coefficient is denoted as the ratio of the 3D hydrodynamic force per unit length to the 2D hydrodynamic force per unit length. The recommended practice of DNV-RP-C205 (DNV 2007) provides close results of several beam-span ratios compared with the formula of Pabst (1930). Meyerhoff (1970) obtained the first numerical results of the added mass of a flat plate with beam-span ratios from 0.1 to 1.0 by using a boundary element method (BEM). The BEM solver is based on a dipole model where the dipoles are distributed on the plate. The results of the BEM calculations were in good agreement with the predictions of Pabst (1930) formula. Baarholm (2005) also calculated the added mass of a flat plate using a more accurate BEM solver based on WAMIT. His-results were also close to the predictions using the formula of Pabst (1930). However, these abovementioned models are not sufficiently accurate for the 3D correction of the water entry of bodies because they were built based on Von Karman (1929) added mass method, which is an original model of the water entry and cannot be used for the transition stage. Beside, they cannot address the effect of deadrise angles on the 3D correction because the added mass model is built on a thin rectangle plate. The second branch is the modeling of the distribution of the hydrodynamic forces on different spanwise sections from the centre to the edge. Garme (2005) proposed a near-transom load model to correct hydrodynamic forces of the near transom sections and his correction function has the form of a hyperbolic tangent function. This model is proposed for the impact between the hull and water surface with a high horizontal speed, such as a trimmed vessel operating at high speed and a seaplane landing on the water surface. The last branch is the studies of the pressure distribution under 3D effects. Smiley (1950) conducted pioneering experiments involving a prismatic model with a deadrise angle of 30° planning on the water surface. An obvious pressure reduction can be observed near the transom section. Both the transverse sections with and without chime immersion have significant 3D effects in the vicinity of the transom section. Zhao et al. (1996) conducted experiments on the water entry of a 3D wedge. Their results unveiled significant pressure reductions on the centre section during the slamming and transition stages. They also developed a BEM (Zhao et al., 1996) to perform the 2D simulation of water entry of a wedge, and the 3D effects of hydrodynamic force and the pressure were revealed. Wang et al. (2021) carried out numerical simulations using OpenFOAM based on a finite volume method (FVM) and show the differences of the pressure distributions between the 2D and 3D water entry for different sections along the spanwise direction. The pressure reductions on the 3D wedge surface due to the 3D effects are closely related to the total hydrodynamic force and the spanwise distribution of the hydrodynamic force. Therefore, the three aspects of the 3D correction should be combined to create a comprehensive picture for the 3D effects of the water entry of bodies.

In the present study, the water entry of 3D wedges is numerically investigated using the FVM combined with the volume of fluid (VOF) method to capture the free surface and the dynamic mesh method of global moving mesh (GMM) (Qu et al., 2015; Wen et al., 2020a). The fluid is considered to be incompressible, non-viscous, weightless and with negligible surface tension effects under the assumption of the high-speed impacts between the wedge and the water. Based on the numerical simulation results, a new model for predicting the total hydrodynamic force, the spanwise hydrodynamic force and the pressure distribution considering the 3D effects is proposed for the first time. This article is organized as follows. The computational approach of FVM with VOF and GMM, and its validations are presented in Section 2. The 3D effects on the total hydrodynamic force, the distribution of hydrodynamic force acting on the spanwise sections and the pressure reductions are theoretically modeled and analyzed in Sections 3 and 4. Finally, the conclusion is given in Section 5.

2. Computational overview

2.1. Model setup

The description of the water entry of a 3D wedge is shown in Fig. 1. The original of an earth-fixed coordinate system is located at the initial contact point where the centre of the keel line impacts the quiescent water surface. The *x*- and *y*-axes are normal to the keel of the wedge in the horizontal and vertical directions, respectively. The z-axis is paralleled to the keel of the wedge in the horizontal direction. The wedge has a beam of $\boldsymbol{l}$ and a spanwise length of $\boldsymbol{L}$.

In the present study, the water entry of 3D wedges with deadrise angles of $\boldsymbol{\beta} = 30$, 35, 40 and 45° and with 6 beam-span ratios of $\boldsymbol{l/L}$ varying from 0.0 to 1.0 are numerically investigated. The case of $\boldsymbol{l/L} = 0.0$ represents the water entry of a 2D wedge where the spanwise length is infinite. The slamming and transition stages are studied. The numerical model is validated against the experimental data reported by Zhao et al. (1996) for the water entry of a 3D wedge with a deadrise angle of $\boldsymbol{\beta} = 30°$ and a beam-span ratio of $\boldsymbol{l/L} = 0.5$.

The gravity effects of the water are neglected under the high-speed impact assumption. The abovementioned deadrise angles are in the range of moderate deadrise angles that the air cushions (Chuang, 1966) and the compressibility effects (Korobkin, 1992) of the water will not be involved. with a negligible gravity effect of fluid for the high-speed water entry problems. The acceleration effects (Wen et al., 2021, 2022b) which are induced by the acceleration of the wedge, are also included in the validation case in Sections 2.3 and 2.4, but not involved the modeling of the 3D effects on the water entry.

2.2. Computational approaches

A FVM with the VOF technique is adopted to provide the detailed results of flow field around the 3D wedge entering the water. The flow is assumed to be incompressible, inviscid and with negligible surface tension effect because of the high-speed water entry. For a slamming problem of a ship, the duration of the water entry process is very small, and the ship hull is usually large. Therefore, the effects of the viscosity and surface tension can be neglected. The assumption was often adopted in the theoretical studies (Wagner, 1932; Howison et al., 1991; Korobkin, 2004; Dobrovol'skaya, 1969; Semenov and Iafrati, 2006; Wen et al., 2020a, 2020b) and BEMs (Zhao et al., 1996; Wu et al., 2004; Zhao and Faltinsen, 1991) for the water entry problems. The GMM method is used to deal with the relative motion between the wedge and the water

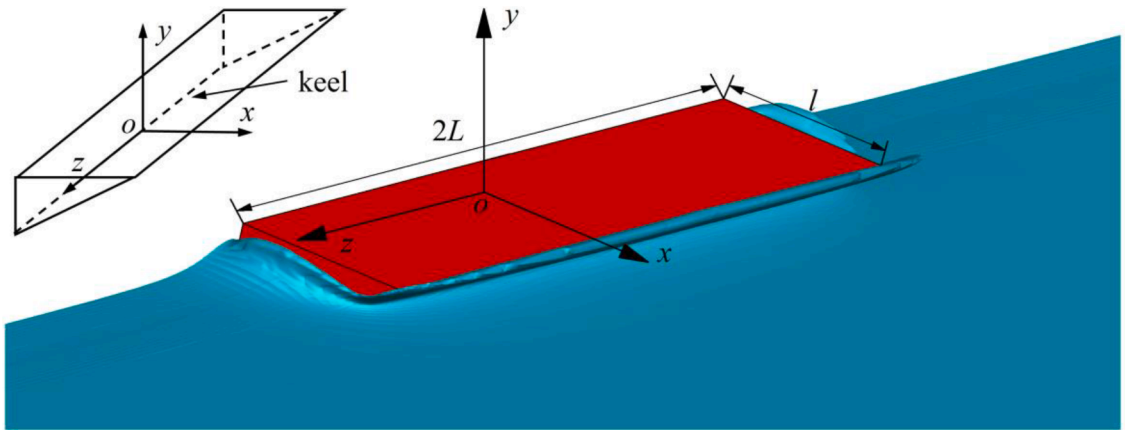

Fig. 1. Description of the water entry of 3D wedge.

surface.

2.2.1. Flow solver

The unsteady incompressible Euler equations ignoring the surface tension force are solved using ANSYS FLUENT as follows.

$$\frac{\partial \boldsymbol{V}}{\partial \boldsymbol{t}} + \boldsymbol{V}\cdot\nabla\boldsymbol{V} = -\frac{1}{\boldsymbol{\rho}}\nabla\boldsymbol{p} - \mathbf{g} \tag{1}$$

where $\boldsymbol{V}$ is the velocity of fluid, $\boldsymbol{\rho}$ is the density, $\boldsymbol{p}$ is the pressure and $\mathbf{g} = (0, -9.81\mathbf{m}/\mathbf{s}^2, 0)$ representing the gravity of fluid. The semi-implicit method for pressure linked equation consistent algorithm (SIMPLEC) is used to deal with the pressure-velocity coupling. The unsteady terms are discretized using a first-order implicit scheme, the convection terms are discretized using a second-order upwind scheme, and the pressure term is discretized using a body force weighted scheme.

2.2.2. VOF method

The VOF method was firstly proposed by Hirt and Nichols (1981), which can capture the free interfaces between two or more immiscible fluids by introducing a variable, called the volume fraction, for each phase. If the volume fraction of the $\boldsymbol{q}^{\mathbf{th}}$ fluid in a certain cell is denoted as $\boldsymbol{c_q}$, represents a cell is empty of the $\boldsymbol{q}^{\mathbf{th}}$ fluid; represents a cell is full of the $\boldsymbol{q}^{\mathbf{th}}$ fluid; and represents the cell containing the interface between the $\boldsymbol{q}^{\mathbf{th}}$ fluid and other fluids. The sum of the volume fractions of all phases must be equal to 1 in each cell. The volume fraction equation of the $\boldsymbol{q}^{\mathbf{th}}$ fluid is written as follows:

$$\frac{\partial}{\partial \boldsymbol{t}}\left(\boldsymbol{c_q}\boldsymbol{\rho_q}\right) + \nabla\cdot\left(\boldsymbol{c_q}\boldsymbol{\rho_q}\boldsymbol{V_q}\right) = 0 \tag{2}$$

where $\boldsymbol{V_q}$ is the velocity of the $\boldsymbol{q}^{\boldsymbol{th}}$ fluid. The first term in the left hand is discretized using one order implicit scheme, and the second term is discretized using a modified high-resolution interface capturing (Modified HRIC) scheme (Muzaferija et al., 1998). The free surface of the water entry of a 3D wedge calculated according to the isosurface of $\boldsymbol{c_q} = 0.5$ for the water is shown in Fig. 1, where the free surface deformations around the 3D wedge are captured well.

2.2.3. GMM method and VOF boundary conditions

In the present study, the global moving mesh method (GMM) (Qu et al., 2015; Wen et al., 2020a) is used to deal with the relative motion between the wedge and the water surface. The whole computational domain (including the cells and boundaries) moves together with the wedge like a rigid body. The motions of the wedge can be prescribed as a given speed history or solved together with Newton's second law.

As the whole computational domain moves, the VOF and the pressure at the far field are updated according to the relative location of the boundary cells with respect to a fixed water level. The volume fraction of water is $\boldsymbol{c_q} = 0.5$ for the cell located on the interface between air and water; $\boldsymbol{c_q} = 0$ for the cells located above the interface; $\boldsymbol{c_q} = 1$ for the cells located below the interface. The pressure is updated similarly.

2.3. Mesh and time-step convergence

Mesh and time-step convergence studies are performed to determine the optimal grid and time-step resolutions. The schematic of the computational domains of the 3D and 2D cases are shown in Fig. 2, and the corresponding boundary conditions are listed in Table 1. A quarter of the model is adopted due to the symmetries of the wedge, which can reduce the computational cost. For the 2D case, an infinite spanwise length $\boldsymbol{L}$ is assumed and thus $\boldsymbol{l}/\boldsymbol{L} = 0.0$. A different grid is adopted for the 2D case. The boundary condition at Plane JIMNDEF is considered as a symmetry and the flow domain outside Plane JIMNDEF is removed. The same spatial resolution of the grid on the wedge surface is adopted. Since the fluid is assumed to be inviscid, incompressible and with negligible surface tension effects, the present approach can produce the same results along the spanwise direction, which can be considered as a 2D water entry. The dimensions of the 3D case domain are set as GH=EK=10$\boldsymbol{l}$, EG=4$\boldsymbol{l}$ and GJ = 12$\boldsymbol{L}$.

The 3D wedge with the deadrise angle of 30° and a beam-span ratio of $\boldsymbol{l}/\boldsymbol{L} = 0.5$ is considered for the mesh and time-step convergence studies, as shown in Fig. 3(a) and (b). The structural mesh details around the wedge are shown in Fig. 3(c). Three sets of meshes with the resolutions from coarse to fine are used and the grid numbers are listed in Table 2. Fig. 4 shows the hydrodynamic forces acting on the wedge surface obtained using the three meshes listed in Table 2 and three time-steps of 2, 4, 8 $\times 10^{-5}$s. The entering speed of the wedge is prescribed as

$$\boldsymbol{U_w} = 6.148 - - 0.8097\boldsymbol{t} - - (30.90\boldsymbol{t})^2 - - (80.25\boldsymbol{t})^3 + (74.70\boldsymbol{t})^4 - - (54.57\boldsymbol{t})^5 \ (\mathbf{m}/\mathbf{s}) \tag{3}$$

using a polynomial of 5 orders from the experimental result obtained using an optical sensor. The results of hydrodynamic forces match well with each other, which verifies the independence of the grid and time-step. Therefore, the grid resolution of Mesh 2 with the time-step of 4 $\times 10^{-5}$ s is adopted for further simulations to achieve a balance between the accuracy of spatial and temporal resolutions and the computational cost. It should be noted that the predicted hydrodynamic force only includes the force acting on the measuring section, which is located at the centre of the wedge and has a span length of 200 mm.

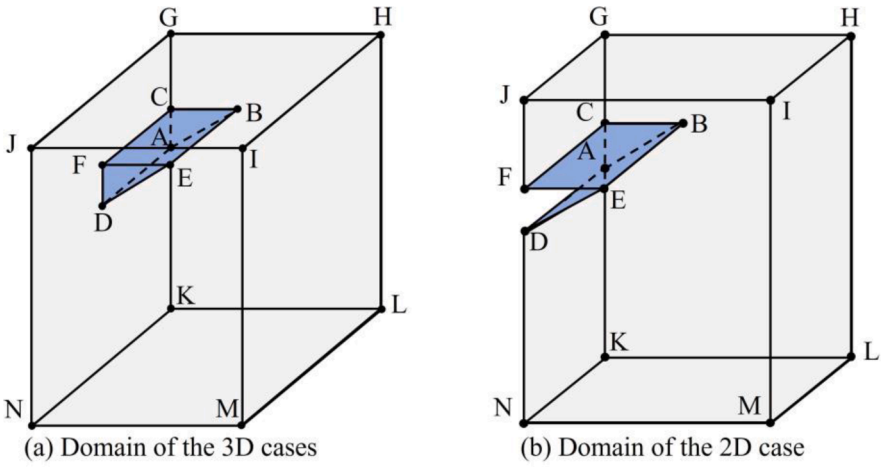

Fig. 2. Schematic of the computational domains of the 3D and 2D cases.

Table 1
Boundary conditions of the water entry of 3D and 2D wedges.

	3D case	2D case
wall	Plane ABED	Plane ABED
	Plane CBEF	Plane CBEF
	Plane DEF	
Symmetry	Plane GHLKABC	Plane GHLKABC
	Plane GCFDAKNJ	Plane GCFJ
		Plane AKND
		Plane JIMNDEF
Pressure-inlet	Plane GHIJ	Plane GHIJ
	Plane KLMN	Plane KLMN
	Plane JIMN	Plane HLMI
	Plane HLMI	

2.3. Validation studies

The validation of the present numerical model is conducted by comparing with the experimental results of Zhao et al. (1996). Fig. 5 shows the comparison of the hydrodynamic forces acting on the wedge surface between the predictions of the present numerical model and the experimental results of Zhao et al. (1996). The results from the present numerical model are in good agreement with the experimental results. Fig. 6 shows the comparisons of the pressure coefficients C_p on the centre section of the wedge between the experimental results of Zhao et al. (1996), the predictions of 2D BEM of Zhao et al. (1996) and the present numerical model. The description of the pressure sensors' locations is illustrated in Fig. 3(b). The results at three different instants are shown: (a) $t = 0.0435$ s; (b) $t = 0.0158$ s; (c) $t = 0.0202$ s. The pressure coefficient is defined as

$$C_p = \frac{p - p_a}{0.5\rho U_w^2} \tag{4}$$

where p_a is the atmospheric pressure. The maximum relative error of 22% happens at the P3 of $t = 0.0202$ s. However, the predictions of the present numerical model are in better agreement with the experimental results than those of the 2D BEM of Zhao et al. (1996) because the 3D effects of the water entry can be well captured by the present 3D numerical simulations. It can be concluded that the present numerical model can accurately predict the hydrodynamic force and pressure acting on the wedge surface for the water entry of wedge in forced motions.

To evaluate the performance of the present method for water entry of wedges in free fall motion, a specific case is conducted. The case involved a wedge with a mass of 60.25 kg (1/4 of the total wedge mass) and an initial entering speed of 6.15 m/s. Fig. 7 displays the comparisons of the hydrodynamic forces acting on the wedge surface, the vertical speed of the wedge between the predictions obtained by the present

Table 2
Details of the three grids used for the mesh convergence studies.

Description	Mesh1 (Coarse)	Mesh2 (Normal)	Mesh3 (Fine)
Cell number	564,073	1749,328	5380,035
Number of nodes on Line AB	59	85	123
Number of nodes on Line AD	55	80	116

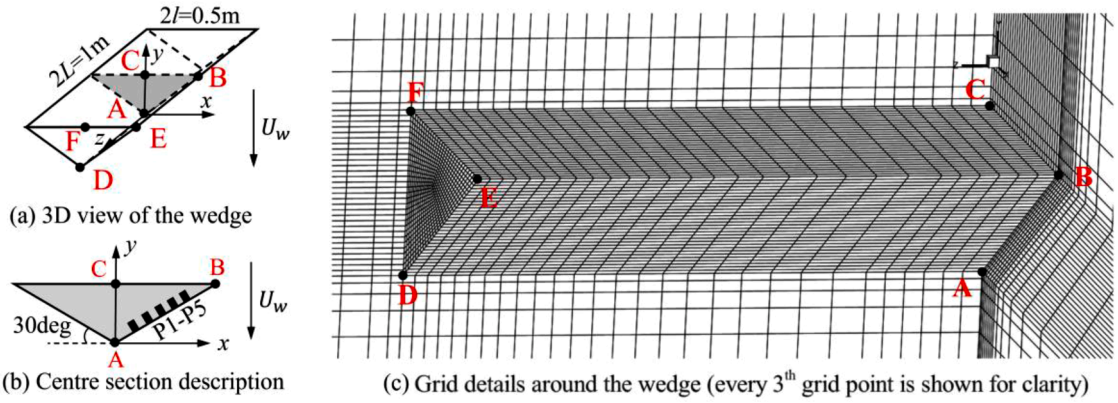

Fig. 3. Description of the 3D wedge (a), centre section (b) and details of the normal grid around the wedge in 1/4 model (c).

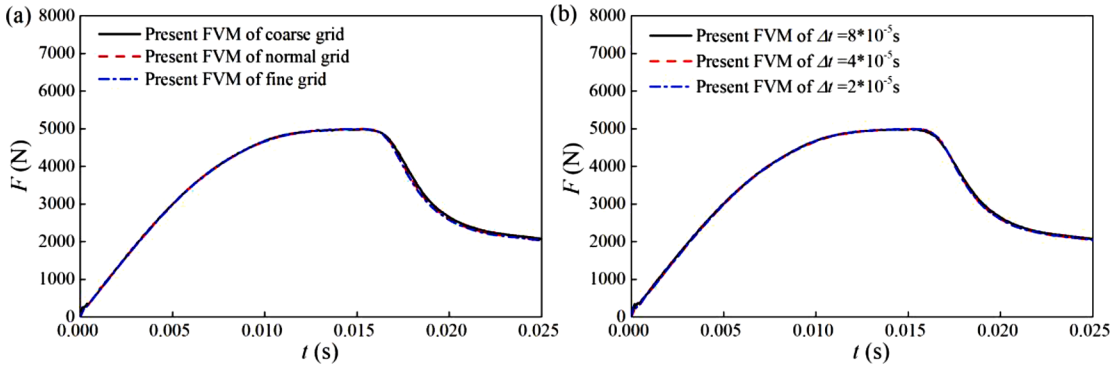

Fig. 4. Mesh (a) and time-step (b) convergence studies of the hydrodynamic forces acting on the wedge surface.

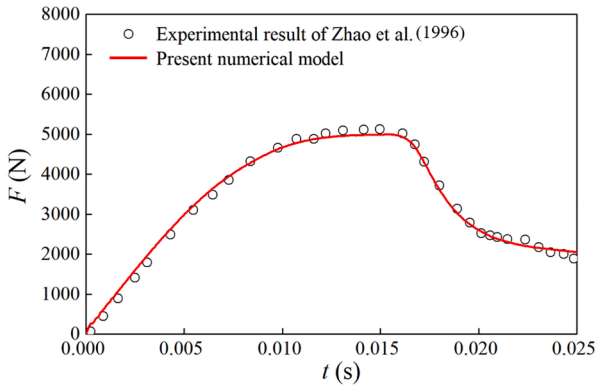

Fig. 5. Comparison of the hydrodynamic forces acting on the wedge surface between the predictions of the present numerical model and the experimental results of Zhao et al. (1996).

numerical model using prescribed speed and considering a free fall motion. The experimental results obtained by Zhao et al. (1996) are also included for comparison. The hydrodynamic force in the free fall motion case is slightly smaller compared to the prescribed speed case, yet it still demonstrates good agreement with the experimental results. Furthermore, the predicted vertical entering speed in the free fall motion case matches the experimental result well.

A comparison of the hydrodynamic force and the wedge speed at 0.015 s between the experimental results of Zhao et al. (1996) and the present FVM is displayed in Table 3. The results show that the present FVM using the prescribed speed has an error of 2.8%, whereas the FVM of the free fall motion yields a slightly higher error of 4%. Additionally, the error in predicting the wedge speed is 0.7%. Therefore, the present numerical model has good predictions of the hydrodynamic force and the wedge motion for both the forced motion and free fall motion cases.

2.4. Case description

For the other cases as described in Section 2.1, the grid of Mesh 2 in Table 1 for $\boldsymbol{\beta} = 30\mathbf{deg}$ and $\boldsymbol{l/L} = 0.5$ is scaled in vertical and span directions to generate the grids of different deadrise angles and beam-span ratios to keep the same grid resolution. The time-step resolution is also kept the same using the following expression for different beam-span ratios and deadrise angles.

$$\frac{\boldsymbol{U_0 \Delta t}}{\boldsymbol{l}} \approx \frac{0.005}{\boldsymbol{C_{s2max}}} \tag{5}$$

$\boldsymbol{C_{s2max}}$ is the maximum slamming coefficient of the water entry of 2D wedges. The adopted time-steps and the total simulation time of different deadrise angles are shown in Table 4, where 2000 time-steps are adopted for all cases.

3. 3D effects on the total hydrodynamic force

In this section, the water entry of 3D wedges with different beam-span ratios is investigated. The entering speed $\boldsymbol{U_0}$ is assumed to be constant and the gravity effect of fluid is negligible due to the high-speed impacts. The 3D effects on the total hydrodynamic fore acting on the wedge surface for the water entry of a wedge are revealed.

3.1. Dimensional analysis of the pressure in the slamming stage

A dimensional analysis is conducted for the pressure $\boldsymbol{p - p_a}$ on the wedge surface in the slamming stage of the water entry of a wedge with the deadrise angle of $\boldsymbol{\beta}$ in a constant speed. The involved variables are the pressure $\boldsymbol{p - p_a}$, the water density $\boldsymbol{\rho}$, the impact speed $\boldsymbol{U_0}$, the penetration depth $\boldsymbol{h}$, the spanwise length $2\boldsymbol{L}$ and the coordinates $\boldsymbol{x}$ and $\boldsymbol{z}$. For the slamming stage, the beam of wedge $2\boldsymbol{l}$ is not involved because the spray root does not reach the knuckle of the wedge. It seems that the impact flow does not "feel" the top of the wedge in this case. Therefore,

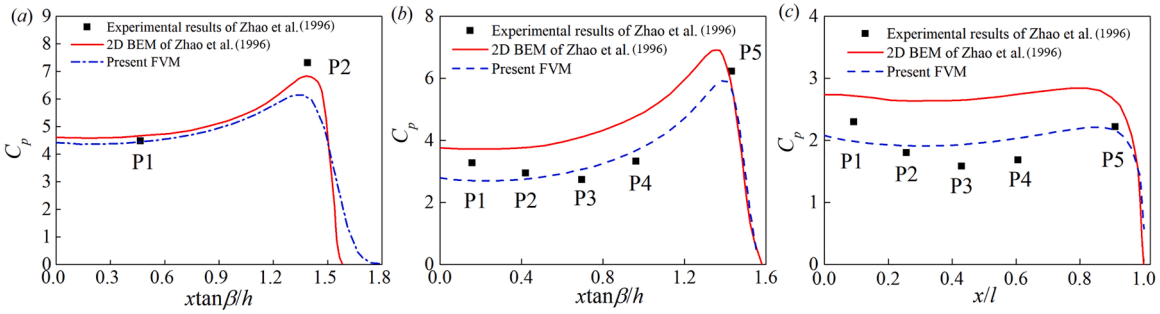

Fig. 6. Comparisons of the pressure coefficients $\boldsymbol{C_p}$ on the centre section of the wedge between the experimental results of Zhao et al. (1996) (see Fig. 3(b) at the pressure sensors P1-P5), the predictions of 2D BEM of Zhao et al. (1996) and the present numerical model. The results of three different instants are shown: (a) $\boldsymbol{t} = 0.0435$ s; (b) $\boldsymbol{t} = 0.0158$ s; (c) $\boldsymbol{t} = 0.0202$ s.

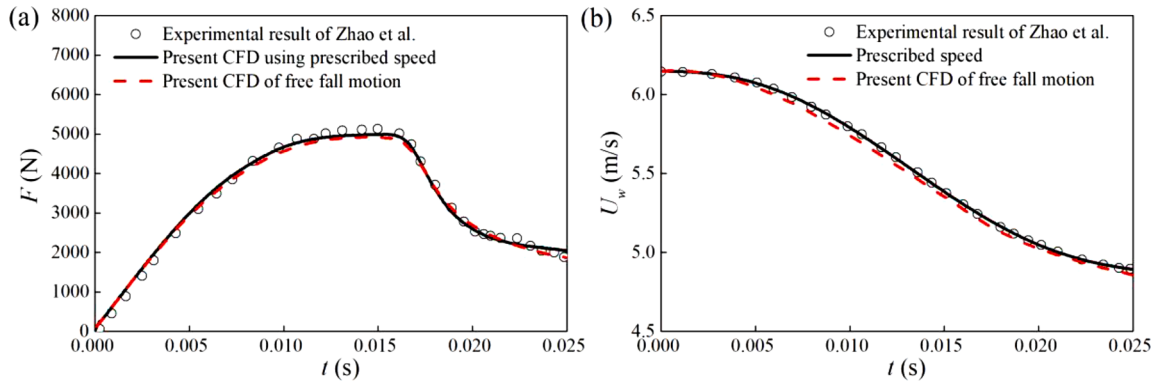

Fig. 7. Comparisons of (a) the hydrodynamic forces acting on the wedge surface and (b) the vertical speed of the wedge between the predictions obtained by the present numerical model using prescribed speed and the results considering free fall motion. The experimental results obtained by Zhao et al. (1996) are also included for comparison.

Table 3
Comparisons of the hydrodynamic force and the wedge speed at 0.015 s.

	Force at 0.015s	Error	Wedge speed at 0.015s	Error
Experimental results of Zhao et al. (1996)	5127N	–	5.385 m/s	–
Present FVM using the prescribed speed	4985N	2.8%	–	–
Present FVM of free fall motion	4920N	4.0%	5.35 m/s	0.7%

Table 4
Time-step and total simulation time of different deadrise angles.

β (°)	30	35	40	45
C_{s2max}	5.0423	3.8119	2.9111	2.2314
h_2/l	0.3710	0.4548	0.5568	0.6760
$U_0\Delta t/l$	1.0×10^{-3}	1.2×10^{-3}	1.6×10^{-3}	2.0×10^{-3}
$U_0 t_{end}/l$	2	2.4	3.2	4

the dimensional analysis for the water entry with a specific deadrise angle of β yields

$$p - p_a = \frac{1}{2}\rho U_0^2 f\left(\frac{x}{c}, \frac{z}{L}, \frac{c}{L}\right) \tag{6}$$

where c is the wetted length of the wedge and is usually adopted to replace the penetration depth h in the slamming stage (Wen et al., 2022a) using the following expression

$$c = \frac{hl}{h_2} \tag{7}$$

where h_2 is the penetration depth corresponding to the maximum slamming coefficient C_{smax}. The total slamming coefficient is defined as

$$C_s = \frac{F}{0.5\rho U_0^2 lL} \tag{8}$$

where F is the total hydrodynamic force of a quarter of the model. The pressure coefficient for the water entry in a constant speed is defined as

$$C_p = \frac{p - p_a}{0.5\rho U_0^2} = f\left(\frac{x}{c}, \frac{z}{L}, \frac{c}{L}\right) \tag{9}$$

Based on Eq. (9), we can set up an expression of the total slamming coefficient of C_s. It should be noted that for $l/L = 0.0$, the problem becomes a 2D water entry and the corresponding C_s is denoted as C_{s2}. By integrating Eq. (9), C_s has the following expression

$$C_s = \frac{c}{l}\iint f(x/c, z/L, c/L)d(x/c)d(z/L) = \frac{c}{l}C\Psi(c/L) \tag{10}$$

where C is a constant and $\Psi(c/L)$ is an unknown function satisfying $\Psi(0) = 1$. By considering $c << L$ at $c = l$, the constant C appears to be the maximum slamming coefficient of a 2D water entry, denoted as C_{s2max}. Then, the slamming coefficient of the water entry of 3D wedges has the following form

$$C_s = \frac{c}{l}C_{s2max}\Psi\left(\frac{c}{L}\right) \tag{11}$$

where $\Psi(c/L)$ can be denoted as a 3D effect coefficient. Thus, the 3D effects of the water entry on the total hydrodynamic force can be absorbed into the changing of the wetted length c and the 3D effect coefficient $\Psi(c/L)$. Furthermore, according to Eq. (7), c is closely related to h_2. Therefore, in Section 3.2, the modeling of h_2 is considered.

3.2. Modeling of the total hydrodynamic force with 3D effects in the slamming stage

To determine Ψ and h_2, the characteristics of the maximum hydrodynamic forces with different beam-span ratios are investigated. Fig. 8 shows the slamming coefficient C_s with different beam-span ratios for the water entry of 3D wedges with $\beta = 30$**deg**. All the cases have an increasing C_s in the slamming stage and a decreasing C_s in the transition stage. There are significant reductions of total hydrodynamic forces compared with the 2D results ($l/L = 0$) in the slamming and transition stages as the beam-span ratio l/L increases. The maximum slamming coefficient C_{smax} and the corresponding penetration depth h_2 with

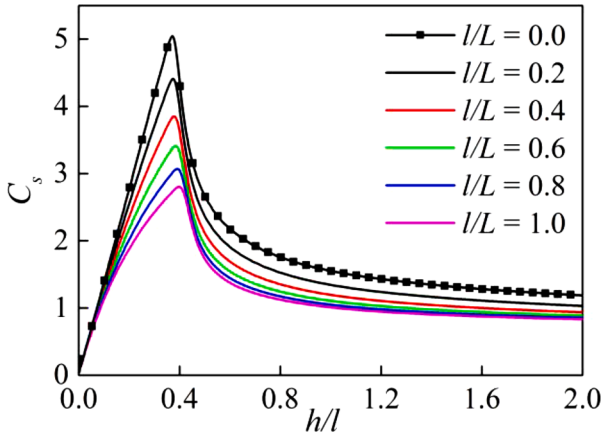

Fig. 8. Slamming coefficients C_s for the water entry of 3D wedges with $\beta = 30°$.

different beam-span ratios are shown in Fig. 9. Two quadratic functions are used to fit the numerical results of the maximum slamming coefficient and the corresponding penetration depth as

$$\Psi\left(\frac{l}{L}\right) = 1 - A\frac{l}{L} + B\frac{l^2}{L^2} \tag{12}$$

$$h_2 = h_{2D}\left(1 + a\frac{l}{L} + b\frac{l^2}{L^2}\right) \tag{13}$$

where $A = 0.6843$, $B = 0.2413$, $a = 0.0404$ and $b = 0.0351$ for the water entry of a wedge with $\beta = 30°$.

The final expression for the total slamming coefficient in the slamming stage is shown as follows.

$$C_s = C_{s2\max}\frac{c}{l}\left(1 - A\frac{c}{L} + B\frac{c^2}{L^2}\right) \tag{14}$$

The $C_{s2\max}$ and h_{2D} are given in Eqs. (15) and (16) from a 2D water entry model by Wen et al. (Wen et al., 2022a),

$$C_{s2\max} = k_1\frac{\pi^3}{4}\left(1 - \frac{4\beta}{3\pi}\right)^2 \cot\beta \tag{15}$$

$$h_{2D} = k_1 l\tan\beta \tag{16}$$

where

$$k_1 = \begin{cases} 2/\pi, & \beta < 15\ \text{deg} \\ 0.203\beta^2 - 013\beta + 0.655, & \beta \geq 15\ \text{deg} \end{cases} \tag{17}$$

Fig. 10 shows the values of $C_{s\max}$ and h_2 for the water entry of 3D wedges with $\beta = 30°$, 35°, 40° and 45°. As the deadrise angle increases, the reduction of the hydrodynamic force slightly decreases. The 3D effect coefficient has a slight increase in the investigated range of deadrise angle from 30° to 45°. Therefore, the deadrise angle effect on the 3D effect coefficient of hydrodynamic force in the slamming stage is relatively small compared with the beam-span ratio l/L. The value of h_2 generally increases with the increasing l/L for all the deadrise angles. The comparisons of the 3D effect coefficient $\Psi(l/L)$ between the formula of Pabst (Pabst, 1930), the suggested formula by DNV (2007), the BEM results of Meyerhoff (1970) and WAMIT (Baarholm, 2005) and the present numerical results are also given. The result of Pabst (1930) is calculated using an analytical formula.

$$\Psi\left(\frac{l}{L}\right) = \frac{1}{\sqrt{1 + \left(\frac{l}{L}\right)^2}}\left[1 - \frac{0.425\frac{l}{L}}{1 + \left(\frac{l}{L}\right)^2}\right] \tag{18}$$

The results of Meyerhoff (Meyerhoff, 1970) and WAMIT (Baarholm, 2005) were given by evaluating the added masses of thin rectangular plates in an infinite fluid using the potential theory. The recommended practice of DNV-RP-C205 (DNV, 2007) provides several results of the 3D effect coefficient for the 3D correction on the added mass of a flat plate. The abovementioned methods have generally close results of the 3D coefficient in the range of $l/L \in [0, 1]$. All these empirical formulas or results from potential theory are based on the 3D effects of the added mass of a flat plate, which cannot predict the difference of Ψ between different deadrise angles. The present study uses quadratic functions to fit the Ψ of different deadrise angles. The fitting coefficients A and B are listed in Table 5. These fitting coefficients together with Eq. (14) can accurately provide the hydrodynamic forces acting on wedge surface with different deadrise angles in the slamming stage.

3.3. Modeling of the total hydrodynamic force with 3D effects in the transition stage

The flow in the transition stage is more complicated than that in the slamming stage. The flow separation and the appearance of the new free surface near the spray root make it difficult to conduct a similar dimensional analysis in Section 3.1 for the transition stage. Instead of proposing a theoretical model of the 3D effect coefficient, a transition stage model similar to that of the 2D model reported by Wen et al. (2022a) is proposed for calculating the slamming coefficient of the water entry of 3D wedges,

$$C_s = C_{s\infty} + C_s^*(C_{s\max} - C_{s\infty}) \tag{19}$$

where

$$C_s^* = \begin{cases} 1, & 0 \leq h^* < 0.067 \\ \dfrac{1.539h^* + 2.168}{h^{*2} + 8.081h^* + 2.169}, & h^* \geq 0.067 \end{cases} \tag{20}$$

and

$$h^* = \frac{h - h_2}{h_2}\cot^{1.3075}\beta \tag{21}$$

are the same with those of 2D model of Wen et al. (2022a). $C_{s\infty}$ is the slamming coefficient of a supercavitating flow around a 3D wedge with a beam-span ratio of l/L. The slamming coefficient of the supercavitating flow around a 2D wedge $C_{s2\infty}$ can be theoretically derived (Korvin-Kroukovsky and Chabrow, 1948; Gurevich, 1965; Wen et al., 2022a). The values of $C_{s2\infty}$ and shown Table 6. The $C_{s\infty}$ for the supercavitating flow around a 3D wedge is difficult to be theoretically calculated because of the 3D effects. Therefore, $C_{s\infty}$ is obtained from the numerical results in the transition stage by comparing the predictions of Eq. (19) and the selected numerical results of $h/h_2 = 5$. It is worth mentioning that the $C_{s\infty}$ cannot be directly calculated using the numerical method because the penetration depth is infinite. The present model can be treated as an approximate model for calculating the value of $C_{s\infty}$.

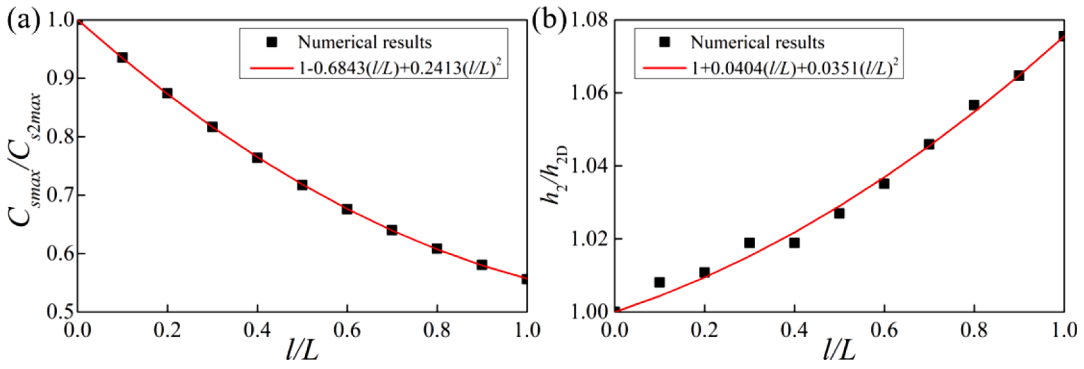

Fig. 9. Maximum slamming coefficient $C_{s\max}$ (a) and the corresponding penetration depth h_2 (b) for the water entry of 3D wedges with $\beta = 30°$.

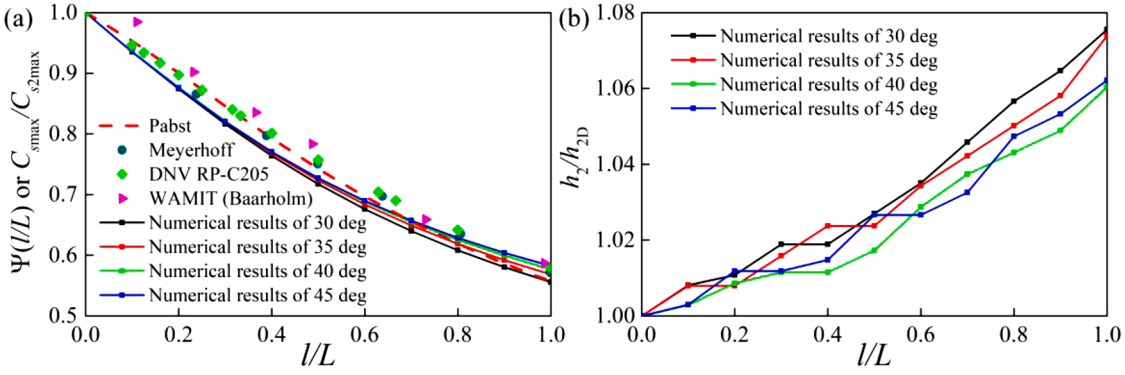

Fig. 10. $C_{s\max}$ (a) and h_2 (b) of the water entry of 3D wedges with $\beta = 30°$, 35°, 40° and 45° in a constant speed. The 3D effect coefficient $\Psi(l/L)$ of the formula of Pabst (1930), the suggested formula by DNV (2007) and the BEM results of Meyerhoff (1970) and WAMIT (Baarholm, 2005) are also included.

Table 5
A and *B* of different deadrise angles.

β (°)	*A*	*B*
30	0.6843	0.2413
35	0.6728	0.2427
40	0.6689	0.2479
45	0.6734	0.2583

Table 6
$C_{s2\infty}$, $C_{s2\infty min}$ and λ of different deadrise angles.

β (°)	$C_{s2\infty}$	$C_{s\infty min}$	$C_{s\infty min}/C_{s2\infty}$	λ
30	0.7448	0.5608	0.7529	8.9514
35	0.7126	0.5230	0.7340	10.2404
40	0.6768	0.4859	0.7179	11.1063
45	0.6370	0.4432	0.6958	11.6326

Fig. 11(a) shows the obtained $C_{s\infty}$ of different deadrise angles and beam-span ratios using the abovementioned method. The values of $C_{s\infty}$ decrease with the increasing l/L in a range of [0, 0.3] and converges to different constant values in a range of [0.3, 1.0] for different deadrise angles. To evaluate the $C_{s\infty}$ and address the effect of deadrise angle, a new variable $C^*_{s\infty}$ is introduced in Eq. (22).

$$C^*_{s\infty} = \frac{C_{s\infty} - C_{s\infty\min}}{C_{s2\infty} - C_{s\infty\min}} \tag{22}$$

where $C_{s\infty\min}$ is the minimum $C_{s\infty}$ in $l/L \in [0, 1]$ and given in Table 6. The variations of $C^*_{s\infty}$ with l/L for different deadrise angles are shown in Fig. 11(b). They become almost the same for different deadrise angles. For simplicity, a fitting function for $C^*_{s\infty}$ can be proposed as

$$C^*_{s\infty} = \frac{1}{1 + (\lambda l/L)^2} \tag{23}$$

The unknown variable λ is given by a regression analysis of $C^*_{s\infty}$ and is also shown in Table 6. An averaged $\lambda = 10.5$ is adopted. Finally, the expression of $C_{s\infty}$ for the supercavitating flow around a 3D wedge is given as follows.

$$C_{s\infty} = \frac{C_{s2\infty} + C_{s\infty\min}(\lambda l/L)^2}{1 + (\lambda l/L)^2} \tag{24}$$

For the transition stage, the 3D effect on the hydrodynamic force can be attributed to the 3D effect coefficient Ψ in Eq. (12) and $C^*_{s\infty}$ in Eq. (23), which are respectively related to $C_{s\max}$ and $C_{s\infty}$ in Eq. (19). The deadrise angle effect on the 3D effect of the hydrodynamic force is already included into the $C_{s2\infty}$ and $C_{s\infty\min}$ in Table 6. Since $C_{s\infty\min}/C_{s2\infty}$ does not significantly change as the deadrise angle increases, the deadrise angle effect on the 3D correction in the transition is also relatively small compared with the effect of the beam-span ratio.

3.4. Comparisons between the present model and the numerical results

In this section, the prediction performance of the proposed model for C_s using Eq. (14) of the slamming stage and Eq. (19) of the transition stage are evaluated against the numerical simulation results. Fig. 12 shows the comparisons of C_s between the numerical results and the present model for the water entry of a wedge with $\beta = 30°$ and different l/L. The predictions of the present model are in good agreement with the numerical results for the slamming and transition stages during the water entry of a wedge $\beta = 30°$. Fig. 13 shows the comparisons of C_s for the water entry of wedges with different deadrise angles and $l/L = 1.0$. The present model works well for the cases with different deadrise angles. Based on these comparisons, it can be proved that the present

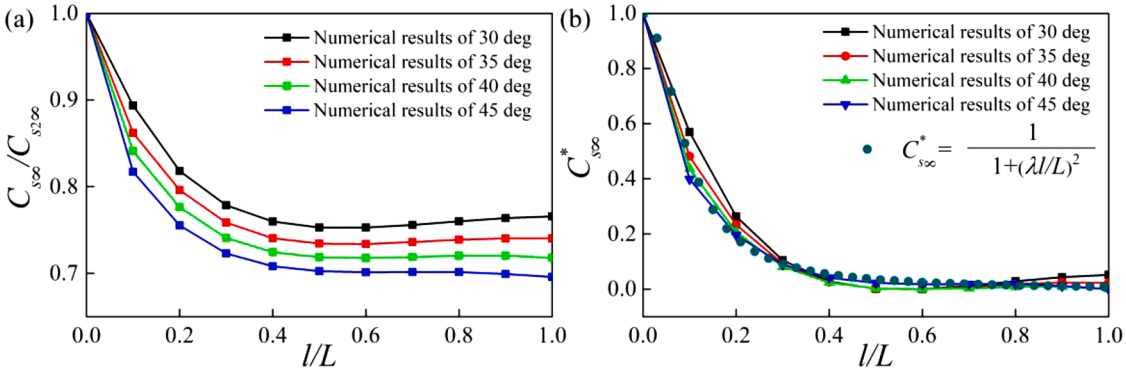

Fig. 11. $C_{s\infty}$ (a) and $C^*_{s\infty}$ (b) of different deadrise angles and beam-span ratios.

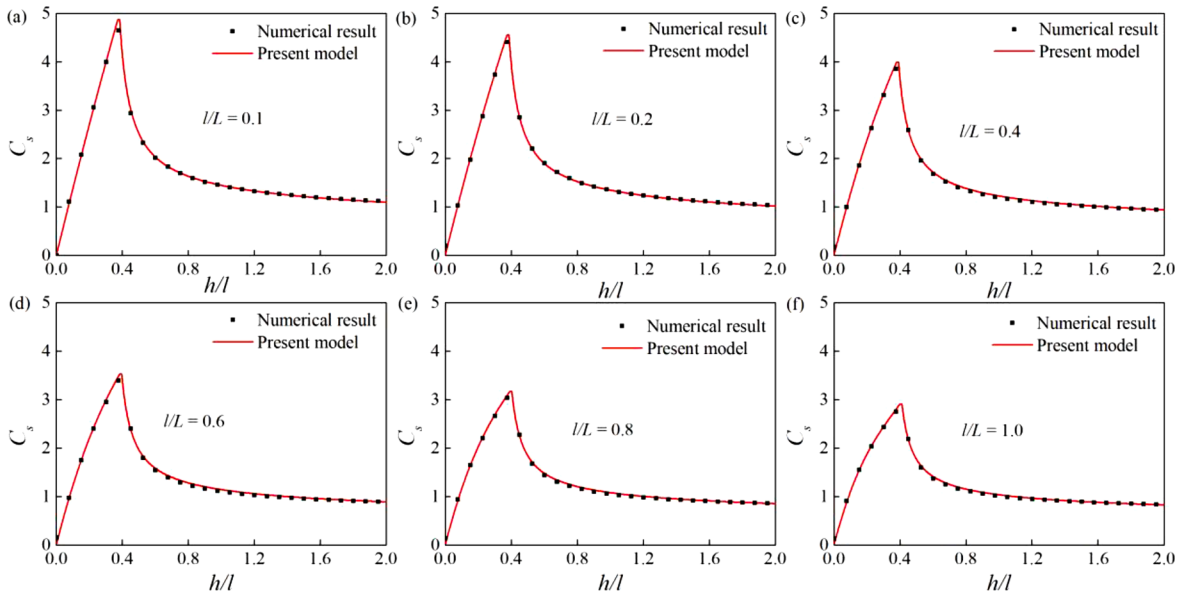

Fig. 12. Comparisons of C_s between the numerical results and the predictions of the present model for the water entry of wedges with $\beta = 30°$ and different l/L.

model works well for the present investigated cases.

4. Three-dimensional effects on the spanwise slamming coefficient and the pressure distribution

The details of the distribution of the spanwise hydrodynamic force and the pressure are investigated. The spanwise force $\mathbf{d}F/\mathbf{d}z$ is the gradient of the total hydrodynamic force along the spanwise direction. A spanwise slamming coefficient is defined from $\mathbf{d}F/\mathbf{d}z$ in Eq. (25)

$$C_{sz} = \frac{\mathbf{d}F}{0.5\rho U_0^2 l \mathbf{d}z} \tag{25}$$

In this section, the spanwise slamming coefficient will be modeled based on the numerical results and the theoretical results of the supercavitating flow around a 2D plate. Then, an approximate model for the pressure reduction due to the 3D effects is proposed.

4.1. Numerical results of spanwise slamming coefficient and its modeling

Figs. 14(a) and 15(a) show the spanwise slamming coefficients C_{sz} of different spanwise sections during the water entry of wedges with $\beta = 30°$ and $l/L = 0.2$ and 1.0. The values of C_{sz} decrease from the centre section to the outer section for both the slamming and transition stages, which is similar to the results of C_s in Fig. 8. The maximum spanwise slamming coefficients C_{szmax} decline dramatically and the penetration depth h_{2z} corresponding to C_{szmax} increases slightly from the centre section to the outer section. Fig. 16 shows the penetration depths h_{2z} corresponding to the maximum C_{smax} of different spanwise sections for the water entry of wedges with $\beta = 30°$, where the results of h_2 of the total hydrodynamic force are also included for comparisons. The value of h_{2z}/l generally increases from the centre section to the edge section from a 2D value of 0.371 (l/L=0) to a maximum value of 0.428 for $l/L = 1.0$. The changes of h_{2z}/l in the range of $l/L \in [0, 1]$ are small and can be neglected. Thus, the values of h_{2z}/l at all spanwise sections can be assumed constant as h_2/l which is the dimensionless penetration depth corresponding to the maximum total hydrodynamic force given in Eq. (13).

Figs. 14(b) and 15(b) show the normalized C_{sz} using the C_{szmax} of different spanwise sections from $l/L = 0.0$ and $l/L = 0.9$. The normalization results of different spanwise sections are found consistent with each other, although there are small discrepancies in the slamming and transition stages. These results also match the normalized C_s using C_{smax}, which indicates that the value of C_s can be used to predict the C_{sz} of all spanwise sections. Fig. 17 shows the distribution of the C_{szmax} for the water entry of wedges with $\beta = 30°$ and different l/L. The value of C_{szmax} decreases with the increasing z/L and l/L. For $z/L = 0$, the results of C_{szmax} are denoted as C_{sz0max}. The values of C_{szmax}/C_{sz0max} of different l/L for the water entry of wedges with $\beta = 30°$ and 45° are shown in Fig. 18. The values of C_{szmax}/C_{sz0max} have a similar distribution along the spanwise direction for $l/L \geq 0.3$. Furthermore, it is also interesting to compare the distributions of C_{szmax}/C_{sz0max} with the C_p distribution of a supercavitating flow around a 2D flat plate, which is a classical solution of a cavity flow problem and has been used for different water entry problems (Korvin-Kroukovsky and Chabrow, 1948; Gurevich, 1965;

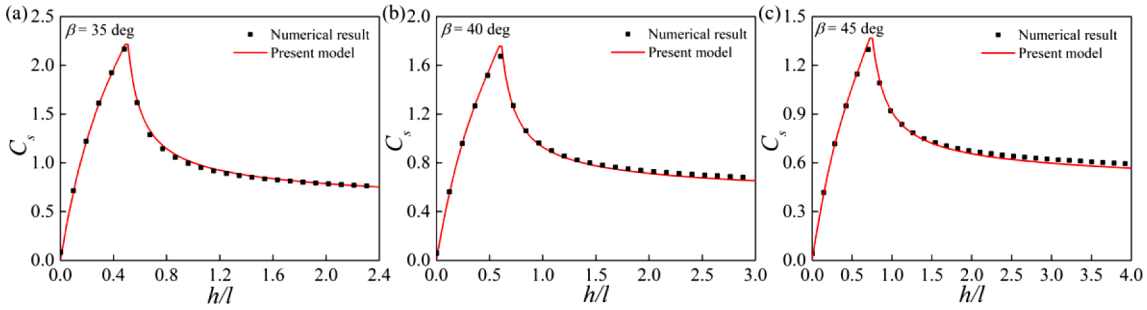

Fig. 13. Comparisons of C_s between the numerical results and the predictions of the present model for the water entry of wedges with deadrise angles of 35° (a), 40° (b) and 45° (c) as well as $l/L = 1.0$.

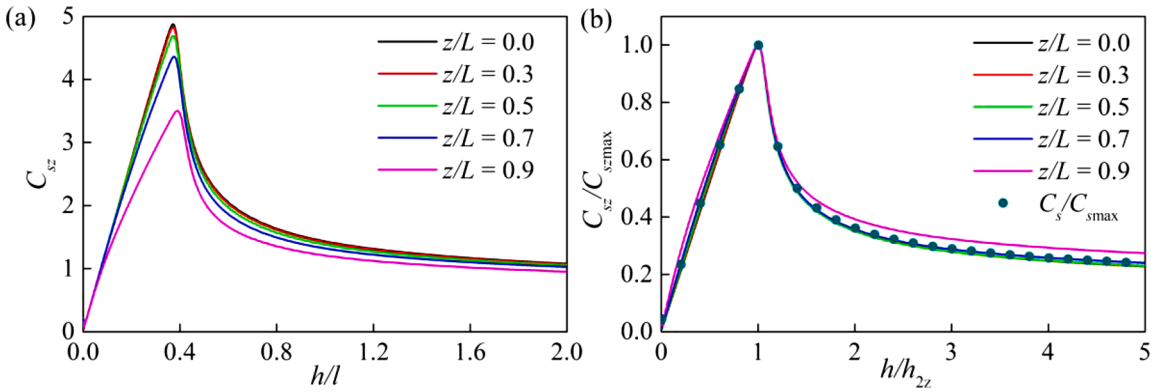

Fig. 14. Spanwise slamming coefficients C_{sz} and normalized C_{sz} using the C_{szmax} of different spanwise sections during the water entry of wedges with $\beta = 30°$ and $l/L = 0.2$.

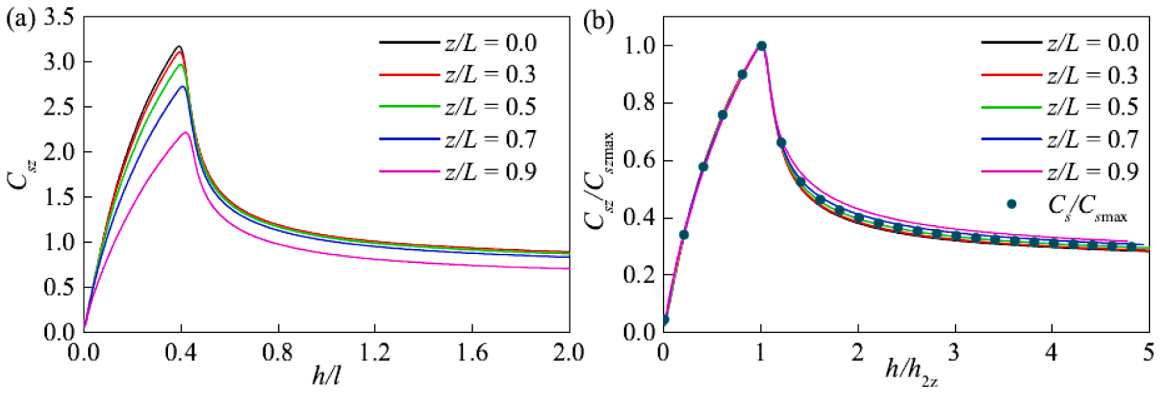

Fig. 15. Spanwise slamming coefficients C_{sz} of different spanwise sections during the water entry of wedges with and $l/L = 1.0$.

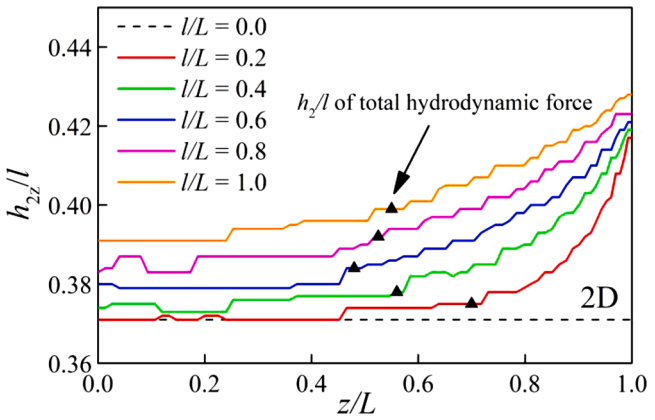

Fig. 16. Penetration depths h_{2z} corresponding to the maximum C_{szmax} of different spanwise sections for the water entry of wedges with $\beta = 30°$, where the results of h_2 (triangles) of the total hydrodynamic force are also included.

Wen et al., 2022a). The theoretical model of the supercavitating flow around a 2D wedge with an arbitrary β is detailed in Appendix, and the case of a flat plate is a particular case with $\beta = 0$. A good agreement can be observed between the C_{szmax}/C_{sz0max} of $l/L \geq 0.3$ and the C_p distribution of a supercavitating flow around a 2D flat plate.

An approximate model for predicting the spanwise slamming coefficient is proposed based on the following assumptions summarized based on the numerical results of C_{sz} from an engineering point of view:

(1) The ratio of the spanwise slamming coefficients C_{sz} and its maximum value is equal to the ratio of the slamming coefficient C_s and the maximum value C_{smax} for different spanwise sections.
(2) h_{2z} of different spanwise sections are equal to h_2 of the total slamming coefficient.
(3) The distribution of C_{szmax}/C_{sz0max} along the spanwise direction can be given by the C_p distribution of a supercavitating flow around a 2D flat plate.

According to Assumption (1), the C_{sz} has the following expression

$$C_{sz} = C_{szmax}\frac{C_s}{C_{smax}} \tag{26}$$

The C_{szmax} is given as

$$C_{szmax} = \theta C_{sz0max} \tag{27}$$

where θ is a function of z/L and l/L. According to Assumption (2), the integral of the C_{szmax} along the spanwise direction yields the C_{smax}. Then the relationship between the C_{smax} and C_{sz0max} is given as

$$C_{smax} = \Theta C_{sz0max} \tag{28}$$

where Θ is a function of l/L defined as

$$\Theta(l/L) = \int_0^1 \theta(z/L, l/L)\mathrm{d}(z/L) \tag{29}$$

The numerical results of Θ are given as C_{smax}/C_{sz0max} and shown in Fig. 19. For all the investigated deadrise angles, the values of Θ decrease from 1 in the range of $l/L \leq 0.3$ and increases slightly in the range of $l/L > 0.3$. The values of Θ of all the investigated deadrise angles are close to

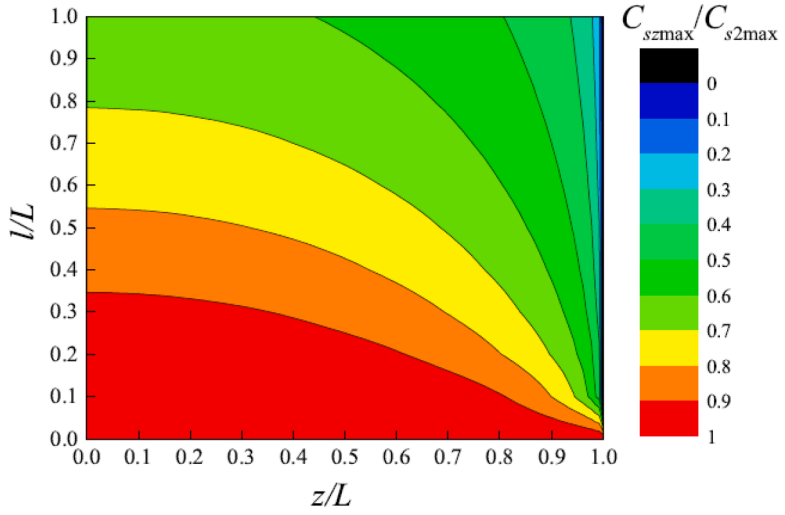

Fig. 17. Distribution of the C_{szmax} for the water entry of wedges with $\beta = 30°$ and different l/L and z/L.

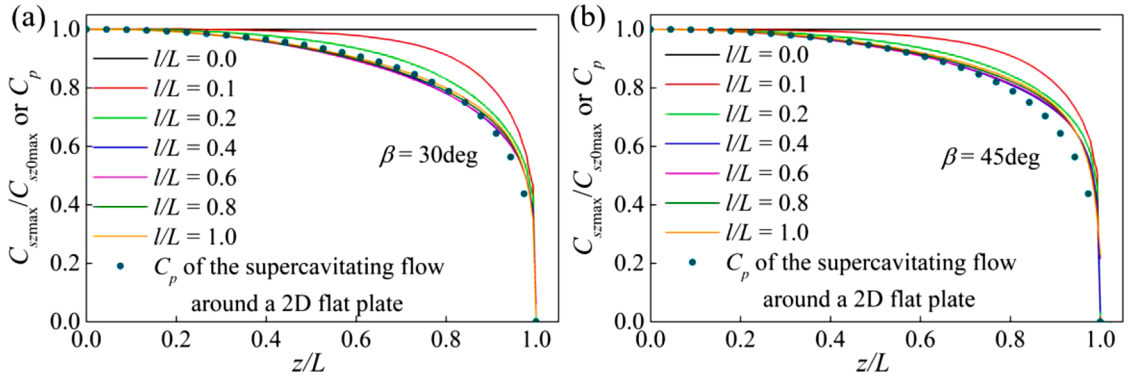

Fig. 18. C_{szmax}/C_{sz0max} of different l/L for the water entry of wedges with $\beta = 30°$ and 45°, where the C_p distribution of the supercavitating flow around a 2D flat plate is given for comparisons.

each other. Based on the similarity of G between different deadrise angles, a similar approximate model to $C^*_{s\infty}$ in Fig. 11(b) for calculating Θ is proposed in Eq. (30)

$$\Theta = \frac{1 + 0.88(\lambda l/L)^2}{1 + (\lambda l/L)^2} \tag{30}$$

where a similar value of λ is also used. The value of 0.88 is obtained from an integral value of the C_p distribution of a supercavitating flow around a 2D flat plate based on Assumption (3). Finally, the expression of C_{sz} has the following form.

$$C_{sz} = C_s \frac{\theta^*}{\Theta} \tag{31}$$

where θ^* is given by Eq. (34) from the C_p distribution of a supercavitating flow of a 2D flat plate in Appendix, and C_s is the total slamming coefficient of the water entry of a 3D wedge calculated using Eqs. (14) and (19). The present model of Eq. (31) is consistent with the expression of total slamming coefficient. It can clearly explain the reduction of C_{sz} due to the increasing beam-span ratio.

Figs. 20 and 21 show the comparisons of C_{sz} between the numerical results and the predictions of the present model for the water entry of 3D wedges with $\beta = 30°$, 45°, $l/L = 0.2$ and 1.0. The present model can generally match the numerical results, especially for the slamming stage. The discrepancies of $l/L = 0.2$ for large z/L in the transition stage are larger than the other cases. The cause of the discrepancies is the errors of Assumption (1) for the outer sections of the wedge as can be seen in Figs. 14 and 15. Therefore, it can be concluded that the present model can accurately predict the spanwise slamming coefficients.

From Eq. (31), the 3D effect on the spanwise slamming coefficient can be divided into two aspects. One is the effect of the beam-span ratio l/L, which affects Θ as shown in Eq. (30) and the total slamming coefficient C_s as shown in Eq. (14). The other one is the effect of spanwise position z/L, given as Eq. (34).

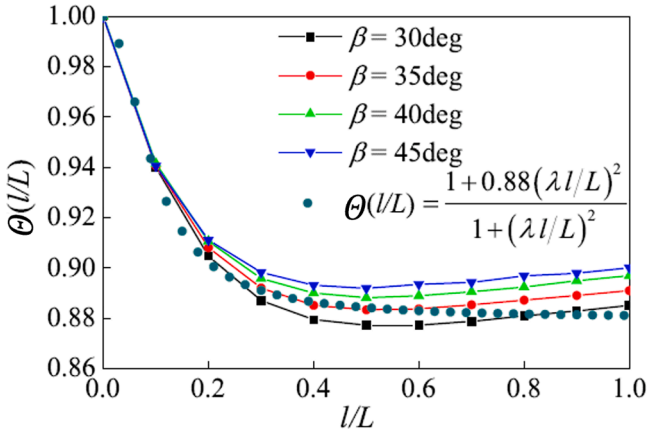

Fig. 19. $\Theta(l/L)$ for the water entry of different deadrise angles.

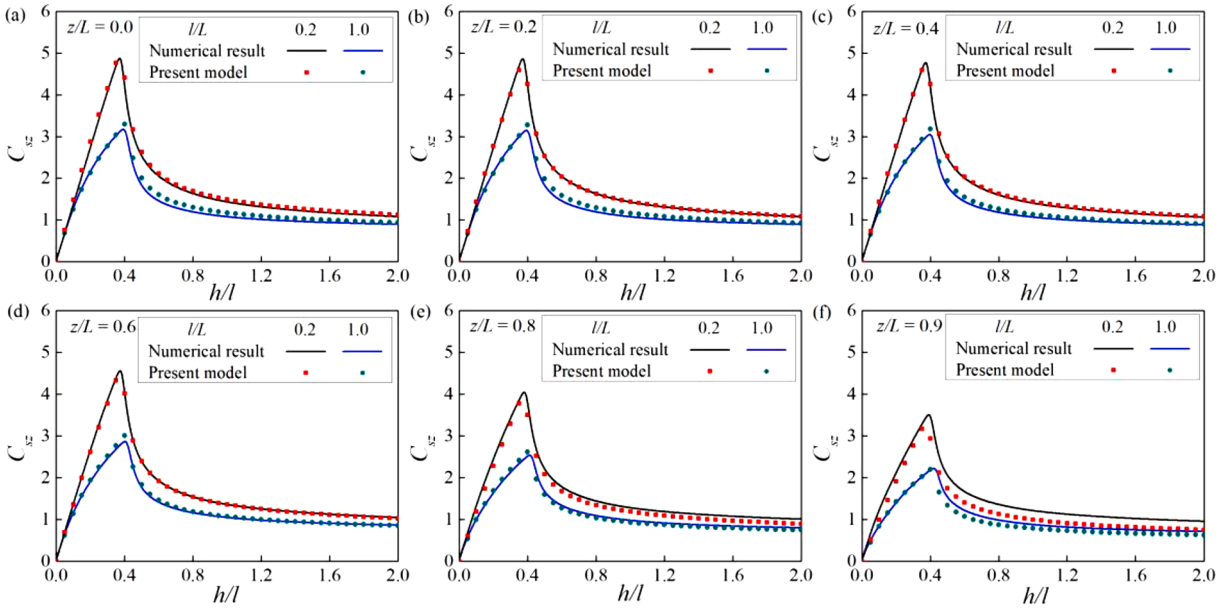

Fig. 20. Comparisons of C_{sz} between the numerical results and the predictions of the present model for the water entry of 3D wedges with $\boldsymbol{\beta} = 30°$, $\boldsymbol{l/L} = 0.2$ and 1.0.

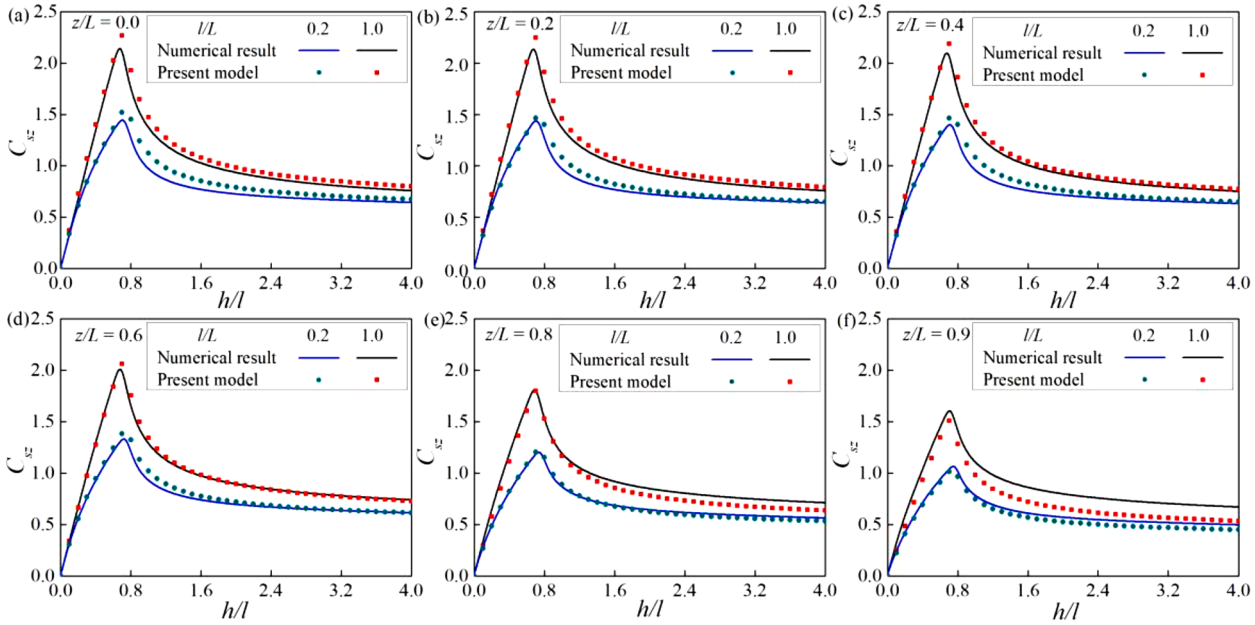

Fig. 21. Comparisons of C_{sz} between the numerical results and the predictions of the present model for the water entry of 3D wedges with $\boldsymbol{\beta} = 45°$, $\boldsymbol{l/L} = 0.2$ and 1.0.

4.2. Three-dimensional effects on the pressure distribution in the slamming stage

Fig. 22(a) shows a comparison of the C_p distributions on the wedge surface of the centre section ($z/L = 0.0$ and $c/l \approx 0.94$) obtained for different beam-ratios during the water entry of 3D wedges with $\boldsymbol{\beta} = 30\mathbf{deg}$. The C_p distributions on the wedge surface have approximately uniform reductions ΔC_p from $x/c = 0$ to 1 for different beam-span ratios, where ΔC_p is the difference of pressure coefficient between the 2D and 3D water entry. It shows that the 3D effects on the pressure distribution in the slamming stage result in an approximately uniform reduction of the pressure coefficient from $x/c = 0$ to 1. Beside, the reductions of C_p increase with the increasing beam-span ratio as shown in Fig. 22(b). Figs. 23(a) and 24(a) show the results of $z/L = 0.5$ and 0.9. The values of ΔC_p of $z/L = 0.5$ are also approximately uniform from $x/c = 0$ to 1. The results of $z/L = 0.9$ have approximately uniform ΔC_p form $x/c = 0$ to 0.85. But ΔC_p dramatically increases from $x/c = 0.85$ to 1. In the present study, the value of ΔC_p is assumed to be constant in $x/c \in [0, 1]$ and can be calculated using the slamming coefficient C_{sz} and C_{s2}

$$\Delta C_p = \frac{l}{c}(C_{s2} - C_{sz}) \tag{32}$$

Combined with Eqs. (11) and (12), the final expression is given as

$$\Delta C_p = C_{s2max}\left[1 - \frac{\theta^*}{\Theta}\left(1 - A\frac{c}{L} + B\frac{c^2}{L^2}\right)\right] \tag{33}$$

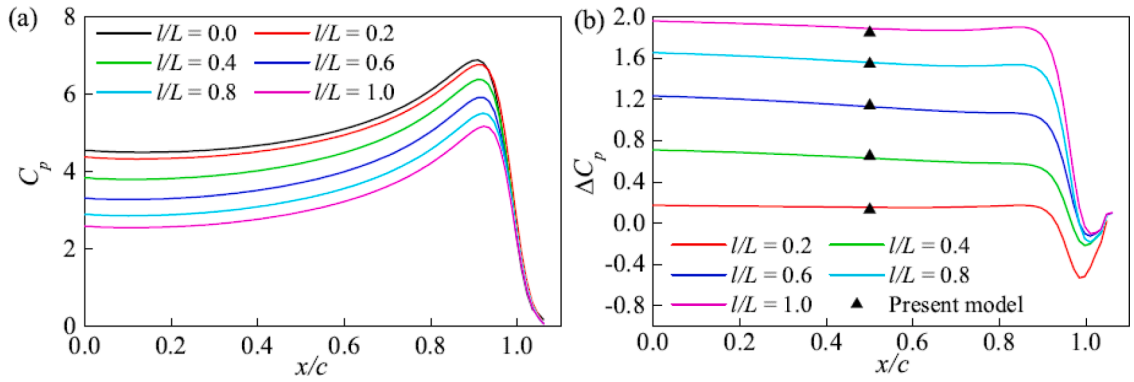

Fig. 22. C_p and ΔC_p on the wedge surface of the centre section ($z/L = 0.0$) between different beam-ratios for the water entry of 3D wedges with $\beta = 30°$. The wetted lengths c/l are close to 0.94.

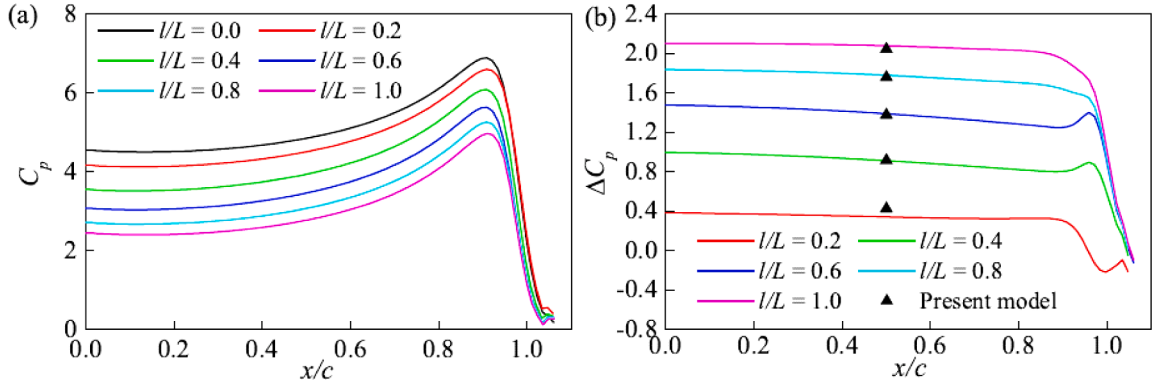

Fig. 23. C_p and ΔC_p on the wedge surface of the section of $z/L = 0.5$ between different beam-ratios for the water entry of 3D wedges with $\beta = 30°$. The wetted lengths c/l are close to 0.94.

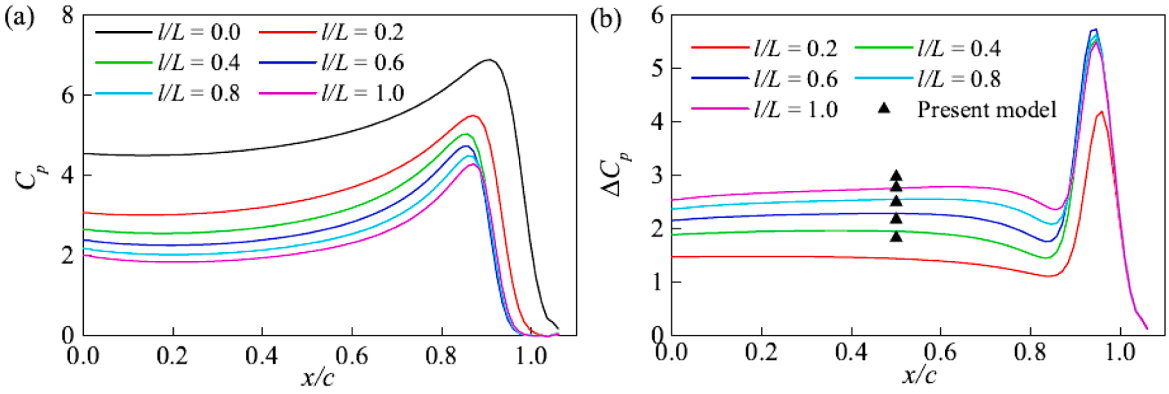

Fig. 24. C_p and ΔC_p on the wedge surface of the section of $z/L = 0.9$ between different beam-ratios for the water entry of 3D wedges with $\beta = 30°$. The wetted lengths c/l are close to 0.94.

Figs. 22(b)–24(b) show the comparisons of ΔC_p between the numerical results and the predictions using Eq. (33) for different beam-span ratios l/L and spanwise sections. The present model is in a good agreement with the numerical results of $z/L = 0.0$ and 0.5. The errors are larger for $z/L = 0.9$ compared with those of $z/L = 0.0$ and 0.5. However, considering that this spanwise section is very close to the edge of the wedge, these errors can be regarded as acceptable for such an approximate model.

5. Conclusions

In the present study, the 3D effects of the water entry of wedges in a constant speed are numerically studied using the FVM combined with the VOF method. The wedge is assumed to enter the water with a high speed such that the compressibility, viscosity, gravity and surface tension effects of fluid can be neglected. The numerical model is validated against an experimental measurement of a freefall water entry of a wedge with a deadrise angle of 30°. The water entry of 3D wedges with deadrise angles of 30, 35, 40 and 45° and with beam-span ratios varying from 0 to 1 are simulated and analyzed. To the author's knowledge, for the first time, the 3D effects on the total and spanwise slamming coefficients and the pressure reductions are modeled in a unified manner for the water entry of 3D bodies. A fast and efficient prediction of these quantities can be achieved using the proposed model. A summary of the

present study on the 3D effects during the water entry of wedges is given as follows:

- For the total slamming coefficient, the expression of the 3D effect coefficient in the slamming stage can be theoretically derived using a dimensional analysis and its parameters are calibrated using the numerical results of the maximum total slamming coefficient. The expression of the total slamming coefficient in the transition stage is extended from a 2D transition stage model. The predictions of the total slamming coefficient in the whole process of water entry of 3D wedges with the deadrise angles from 30 to 45° and with the beam-span ratios from 0 to 1 match well with the numerical results obtained by the FVM.
- For the spanwise slamming coefficients, they are close to the total slamming coefficient normalized by the maximum values. The distribution of the maximum spanwise slamming coefficient can be given by the C_p distribution of a supercavitating flow around a 2D flat plate. An approximate model is proposed and the prediction results are in a good agreement with the FVM results for different deadrise angles, beam-span ratios and spanwise sections.
- For the pressure distribution of different spanwise sections in the slamming stage, the reductions of pressure are approximately constant on the wetted wedge surface and the reduction can be predicted based on the abovementioned expressions of the total slamming coefficient and the spanwise slamming coefficient.

The present 3D correction is based on the results of the water entry of wedges in a constant speed, where the gravity effect of the water and the acceleration effect of the wedge are not included. In further studies, we will attempt to clarify these two effects, and implement the present 3D correction to the strip theory or 2D+t theory to accurately predict the slamming forces and pressure acting on the ships under rough sea conditions.

CRediT authorship contribution statement

Xueliang Wen: Conceptualization, Formal analysis, Investigation, Methodology, Software, Validation, Visualization, Data curation, Writing – original draft, Writing – review & editing. **Muk Chen Ong:** Conceptualization, Investigation, Methodology, Supervision, Resources, Writing – review & editing. **Guang Yin:** Conceptualization, Formal analysis, Investigation, Methodology, Supervision, Writing – review & editing.

Declaration of Competing Interest

The authors declare that they have no known competing financial interests or personal relationships that could have appeared to influence the work reported in this paper.

Data availability

Data will be made available on request.

Appendix A. Supercavitating flow around a 2D linear wedge

The derivations of the supercavitating flow around a 2D linear wedge were given in detail by Wen et al. (2022a). In this section, the key equations for calculating $C_{s2\infty}$ in Section 3.2 are provided. The pressure coefficient on the wedge surface is given as

$$C_p = 1 - \left(\frac{1-\sqrt{1-\tau^2}}{\tau}\right)^{2\left(1-\frac{2\beta}{\pi}\right)} \tag{34}$$

where τ is related to x using the following equation

$$x = \frac{l}{A_0}\int_0^{\tau}\left(\frac{1-\sqrt{1-\tau_0^2}}{\tau_0}\right)^{1-\frac{2\beta}{\pi}}\tau_0 d\tau_0 \tag{35}$$

and

$$A_0 = \int_0^{1}\left(\frac{1-\sqrt{1-\tau_0^2}}{\tau_0}\right)^{1-\frac{2\beta}{\pi}}\tau_0 d\tau_0 \tag{36}$$

The value of $C_{s2\infty}$ can be integrated from Eq. (34).

References

Baarholm, R., 2005. A simple numerical method for evaluation of water impact loads on decks of large-volume offshore platforms. In: Proceedings of the International Conference on Offshore Mechanics and Arctic Engineering, 41952, pp. 203–211.

Chuang, Sheng-Lun, 1966. Experiments on flat-bottom slamming. J. Ship Res. 10, 10–17, 01.

DNV, Environmental conditions and environmental loads, DNV Recommended Practice, DNV-RP-C205 (2007).

D.obrovol'skaya, Z.N., 1969. On some problems of similarity flow of fluid with a free surface. J. Fluid Mech. 36 (4), 805–829.

Faltinsen, O.M., 2005. Hydrodynamics of High-Speed Marine Vehicles. Cambridge University Press, Cambridge, England, pp. 342–388. Chap.IX.

Garme, K., 2005. Improved time domain simulation of planing hulls in waves by correction of the near-transom lift. Int. Shipbuild. Prog. 52 (3), 201–230.

Greenhow, M., Lin. W.M. Nonlinear free surface effects: experiments and theory, Massachusetts Inst of Tech Cambridge Dept of Ocean Engineering: Report No. 83-19 (1983), Massachusetts, USA.

G.urevich, M.I., 1965. The Theory of Jets in an Ideal Fluid. Pergamon Press, Oxford, UK, pp. 1–36. Chap.I.

H.irt, C.W., N.ichols, B.D., 1981. Volume of fluid (VOF) method for the dynamics of free boundaries. J. Comput. Phys. 39 (1), 201–225.

H.owison, S.D., O.ckendon, J.R., W.ilson, S.K., 1991. Incompressible water-entry problems at small deadrise angles. J. Fluid Mech. 222, 215–230.

Kapsenberg, G., 2011. Slamming of ships: where are we now? Philos. Trans. R. Soc. Lond. A Math. Phys. Eng. Sci. 369, 2892–2919.

K.orobkin, A.A., 1992. Blunt-body impact on a compressible liquid surface. J. Fluid Mech. 244, 437–453.

Korobkin, A., 2004. Analytical models of water impact. Eur. J. Appl. Math. 15 (6), 821–838.

Korvin-Kroukovsky, B., Chabrow, F.R., 1948. The Discontinuous Fluid Flow Past an Immersed Wedge. Stevens Institute of Technology, Hoboken New Yersey. , Davidson LaboratoryExperimental Towing tank, Report SITDL-48-9-334Oct.
Luo, H., Wang, H., S.oares, C.G., 2012. Numerical and experimental study of hydrodynamic impact and elastic response of one free-drop wedge with stiffened panels. Ocean Eng. 40 (1), 1–14.
M.eyerhoff, W.K., 1970. Added masses of thin rectangular plates calculated from potential theory. J. Ship Res. 14 (02), 100–111.
Muzaferija, S., Peric, M., Sames, P., Schellin, T., 1998. A two-fluid Navier-Stokes solver to simulate water entry. In: Proceedings of 22nd Symposium on Naval Architecture. National Academy Press, pp. 277–289.
Pabst, W., 1930. Theory of the Landing Impact of Seaplanes. National Advisory Council for Aeronautics (NACA) Technical Memorandum, Washington, USA. No.580.
Qu, Q., Hu, M., Guo, H., Liu, P., A.garwal, R.K., 2015. Study of ditching characteristics of transport aircraft by global moving mesh method. J. Aircr. 52 (5), 1550–1558.
Savitsky, D., DeLorme, M., Datla, R., 2007. Inclusion of whisker spray drag in performance prediction method for high-speed planing hulls. Mar. Technol. 44, 35–56.
Savitsky, D., 1964. Hydrodynamic design of planing hulls. Mar. Technol. SNAME News 1, 71–95.
Semenov, Y.A., Iafrati, A., 2006. On the nonlinear water entry problem of asymmetric wedges. J. Fluid Mech. 547, 231–256.
Smiley, R.F. A study of water pressure distribution during landings with special reference to a prismatic model having a heavy beam loading and a 30 Degree angle of dead rise. National Advisory Council For Aeronautics (NACA) Technical Note No. NACA-TN-2111. Langley Field, VA, USA, (1950).
Sun, H., F.altinsen, O.M., 2007. The influence of gravity on the performance of planing vessels in calm water. J. Eng. Math. 58 (1–4), 91–107.
Sun, H., F.altinsen, O.M., 2012. Hydrodynamic forces on a semi-displacement ship at high speed. Appl. Ocean Res. 34 (none), 68–77.
S.un, S.Y., S.un, S.L., W.u, G.X., 2015. Oblique water entry of a wedge into waves with gravity effect. J. Fluids Struct. 52, 49–64.
Tassin, A., Korobkin, A.A., Cooker, M.J., 2014. On analytical models of vertical water entry of a symmetric body with separation and cavity initiation. Appl. Ocean Res. 48, 33–41.
Von Karman, T. The impact on seaplane floats during landing, National Advisory Council For Aeronautics (NACA) Technical Note 321, Langley Field, VA, USA (1929).
Wagner, H., 1932. Über stoß-und Gleitvorgänge an der Oberfläche von Flüssigkeiten. ZAMM J. Appl. Math. Mech. Z. Angew. Math. Mech. 12 (4), 193–215.
Wang, J., Lugni, C., F.altinsen, O.M., 2015. Experimental and numerical investigation of a freefall wedge vertically entering the water surface. Appl. Ocean Res. 51, 181–203.
Wang, S., Xiang, G., S.oares, C.G., 2021. Assessment of three-dimensional effects on slamming load predictions using OpenFOAM. Appl. Ocean Res. 112, 102646.
Wen, X., Liu, P., Qu, Q., Hu, T., 2020a. Impact of wedge bodies on wedge-shaped water surface with varying speed. J. Fluids Struct. 92, 102831.
Wen, X., Liu, P., Qu, Q., Hu, T., 2020b. Impact of a plate on an asymmetric water wedge. J. Fluids Eng. 142 (4), 041301. Transactions of the ASME.
Wen, X., Liu, P., Qu, Q., Hu, T., 2021. Numerical and theoretical study on the varying speed impact of wedge bodies on a water surface. J. Fluids Eng. 143 (1), 011201. Transactions of the ASME.
Wen, X., Liu, P., Del Buono, A., Qu, Q., Iafrati, A., 2022a. Formulations of hydrodynamic force in the transition stage of the water entry of linear wedges with constant and varying speeds. J. Fluids Struct. 115, 103759.
Wen, X., Del Buono, A., Liu, P., Qu, Q., Iafrati, A., 2022b. Acceleration effects in slamming and transition stages for the water entry of curved wedges with a varying speed. Appl. Ocean Res. 128, 103294.
Wu, G., Sun, H., He, Y., 2004. Numerical simulation and experimental study of water entry of a wedge in free fall motion. J. Fluids Struct. 19 (3), 277–289.
Xie, H., Ren, H., Deng, B., Tang, H., 2018. Experimental drop test investigation into slamming loads on a truncated 3d bow flare model. Ocean Eng. 169, 567–585.
Xie, H., Ren, H., Li, H., Tao, K., 2019. Quantitative analysis of hydroelastic characters for one segment of hull structure entering into water. Ocean Eng. 173, 469–490.
Yettou, E.M., Desrochers, A., Champoux, Y., 2006. Experimental study on the water impact of a symmetrical wedge. Fluid Dyn. Res. 38 (1), 47.
Zekri, H.J., Korobkin, A.A., Cooker, M.J., 2021. Gravity effect on water entry during an early stage. J. Fluid Mech. 916, A10.
Zhao, R., F.altinsen, O.M., 1991. Water entry of two-dimensional bodies. J. Fluid Mech. 246, 593–612.
Zhao, R., F.altinsen, O.M., Aarsnes, J., 1996. Water entry of arbitrary two- dimensional sections with and without flow separation. In: Proceedings of the 21st Symposium on Naval Hydrodynamics. National Academy Press, Trondheim, Norway, pp. 408–423.